

Don't take it lightly: Phasing optical random projections with unknown operators

Sidharth Gupta*, Rémi Gribonval[†], Laurent Daudet[‡] and Ivan Dokmanić*

*University of Illinois at Urbana-Champaign, [†]Inria Rennes - Bretagne Atlantique, [‡]LightOn
 gupta67@illinois.edu, remi.gribonval@inria.fr,
 laurent@lighton.io, dokmanic@illinois.edu

July 4, 2019

Abstract

In this paper we tackle the problem of recovering the phase of complex linear measurements when only magnitude information is available and we control the input. We are motivated by the recent development of dedicated optics-based hardware for rapid random projections which leverages the propagation of light in random media. A signal of interest $\boldsymbol{\xi} \in \mathbb{R}^N$ is mixed by a random scattering medium to compute the projection $\boldsymbol{y} = \boldsymbol{A}\boldsymbol{\xi}$, with $\boldsymbol{A} \in \mathbb{C}^{M \times N}$ being a realization of a standard complex Gaussian iid random matrix. Two difficulties arise in this scheme: only the intensity $|\boldsymbol{y}|^2$ can be recorded by the camera, and the transmission matrix \boldsymbol{A} is unknown. We show that even without knowing \boldsymbol{A} , we can recover the unknown phase of \boldsymbol{y} for some *equivalent* transmission matrix with the same distribution as \boldsymbol{A} . Our method is based on two observations: first, changing the phase of any row of \boldsymbol{A} does not change its distribution; and second, since we control the input we can interfere $\boldsymbol{\xi}$ with arbitrary reference signals. We show how to leverage these observations to cast the *measurement* phase retrieval problem as a Euclidean distance geometry problem. We demonstrate appealing properties of the proposed algorithm on both numerical simulations and in real hardware experiments. Not only does our algorithm accurately recover the missing phase, but it mitigates the effects of quantization and the sensitivity threshold, thus also improving the measured magnitudes.

1 Introduction

Random projections are at the heart of many algorithms in machine learning, signal processing and numerical linear algebra. Recent developments ranging from classification with random features [16], kernel approximation [24] and sketching for matrix optimization [23, 26], to sublinear-complexity transforms [25] and randomized linear algebra are all enabled by random projections. Computing random projections for realistic signals such as images, videos, and modern big data streams is computation- and memory-intensive. Thus, from a practical point of view, any increase in the size and speed at which one can do the required processing is highly desirable.

This fact has motivated work on using dedicated hardware based on physics rather than traditional CPU and GPU computation to obtain random projections. A notable example is scattering of light

in random media (Figure 1 (left)) with an optical processing unit (OPU). The OPU enables rapid (20 kHz) projections of high-dimensional data such as images, with input dimension scaling up to one million and output dimension also in the million range. It works by “imprinting” the input data $\boldsymbol{\xi} \in \mathbb{R}^N$ onto a coherent light beam using a digital micro-mirror device (DMD) and shining the modulated light through a multiple scattering medium such as titanium dioxide white paint. The scattered lightfield in the sensor plane can then be written as

$$\mathbf{y} = \mathbf{A}\boldsymbol{\xi}$$

where $\mathbf{A} \in \mathbb{C}^{M \times N}$ is the transmission matrix of the random medium with desirable properties.

One of the major challenges associated with this approach is that \mathbf{A} is in general *unknown*. Though it could in principle be learned via calibration [6], such a procedure is slow and inconvenient, especially at high resolution. On the other hand, the system can be designed in such a way that the distribution of \mathbf{A} is approximately iid standard complex Gaussian. Luckily, this fact alone is sufficient for many algorithms and the actual values of \mathbf{A} are not required.

Another challenge is that common light sensors are only sensitive to intensity, and so we can only measure the intensity of scattered light, $|\mathbf{y}|^2$, where $|\cdot|$ is the elementwise absolute value. The phase information is thus lost. While the use of interferometric measurements with a reference could enable estimating the phase, the practical setup is complicated and sensitive and it does not share the convenience and simplicity of the one illustrated in Figure 1 (left).

This motivates us to consider the *measurement phase retrieval (MPR) problem*. The MPR sensor data is modeled as

$$\mathbf{b} = |\mathbf{y}|^2 + \boldsymbol{\eta} = |\mathbf{A}\boldsymbol{\xi}|^2 + \boldsymbol{\eta}, \quad (1)$$

where $\mathbf{b} \in \mathbb{R}^M$, $\boldsymbol{\xi} \in \mathbb{R}^N$, $\mathbf{A} \in \mathbb{C}^{M \times N}$, $\mathbf{y} \in \mathbb{C}^M$, and $\boldsymbol{\eta} \in \mathbb{R}^M$ is noise. The goal is to recover the phase of each complex-valued element of \mathbf{y} , y_i for $1 \leq i \leq M$, from its magnitude measurements \mathbf{b} when $\boldsymbol{\xi}$ is *known* and the entries of \mathbf{A} are *unknown*. The classical phase retrieval problem which has received much attention over the last decade [15, 4] has the same quadratic form as (1) but with a known \mathbf{A} and the task being to recover $\boldsymbol{\xi}$ instead of \mathbf{y} . While at a glance it might seem that not knowing \mathbf{A} precludes computing the phase of $\mathbf{A}\boldsymbol{\xi}$, we show in this paper that it is in fact possible via an exercise in distance geometry.

The noise $\boldsymbol{\eta}$ is primarily due to quantization because standard camera sensors can only measure in low precision, unsigned 8-bit values in our case (integers between 0 and 255 inclusive). Furthermore, cameras may perform poorly at low intensities which is another data-dependent noise source and is modelled in (2) by a binary mask vector $\mathbf{w} \in \mathbb{R}^M$ which is zero when the intensity is below some threshold and one otherwise; \odot denotes the elementwise product.

$$\mathbf{b} = \mathbf{w} \odot (|\mathbf{y}|^2 + \boldsymbol{\eta}) = \mathbf{w} \odot (|\mathbf{A}\boldsymbol{\xi}|^2 + \boldsymbol{\eta}) \quad (2)$$

The distribution of \mathbf{A} follows from the properties of random scattering media [14, 6]. It follows an iid standard complex Gaussian distribution, that is $a_{mn} \sim \mathcal{N}(0, 1) + j\mathcal{N}(0, 1)$ iid for all $1 \leq m, n \leq M, N$.

The usefulness of phase is obvious. While in some applications having only the magnitude of the random projection is enough (see [17] for an example related to elliptic kernels), most applications require the phase. For example, with the phase one can implement a more diverse range of kernels as well as randomized linear algebra routines like randomized singular value decomposition (SVD). We report the results of the latter on real hardware in Section 3.1.

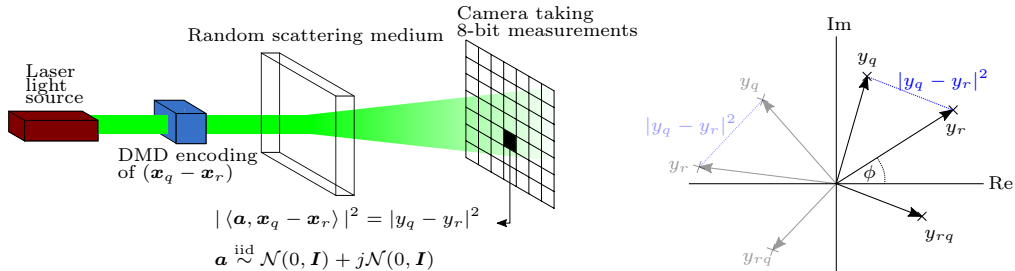


Figure 1: Left: The optical processing unit (OPU) is an example application of where the MPR problem appears. A coherent laser beam spatially encodes a signal $(\mathbf{x}_j - \mathbf{x}_l)$ via a digital micro-mirror device (DMD) which is then shined through random media. A camera measures the squared magnitude of the scattered light which is equivalent to the Euclidean distance between complex numbers $y_q \in \mathbb{C}$ and $y_r \in \mathbb{C}$. Furthermore the camera takes quantized measurements; Right: y_q and y_r are points on the two-dimensional complex plane. We can measure the squared Euclidean distance between points and use these distances to localize points on the complex plane and obtain their phase. Note that rigid body transformations such as rotations and reflections do not change the distances.

Our contributions. We develop an algorithm based on distance geometry to solve the MPR problem (1). We exploit the fact that we control the input to the system, which allows us to mix ξ with arbitrary reference inputs. By interpreting each pixel value as a point in the complex plane, this leads to a formulation of the MPR problem as a pure distance geometry problem (see Section 2.2 and Figure 1) (right). With enough pairwise distances (corresponding to reference signals) we can localize the points on the complex plane via a variant of multidimensional scaling (MDS) [22, 5], and thus compute the missing phase.

As we demonstrate, the proposed algorithm not only accurately recovers the phase, but also improves the number of useful bits of the magnitude information thanks to the multiple views. Established Euclidean distance geometry bounds imply that even with many distances below the sensitivity threshold and coarse quantization, the proposed algorithm allows for accurate recovery. This fact, which we verify experimentally, could have bearing on the design of future random projectors by navigating the tradeoff between physics and computation.

1.1 Related work

The classical phase retrieval problem looks at the case where \mathbf{A} is known and ξ has to be recovered from \mathbf{b} in (1) [7, 20, 10]. A modified version of the classical problem known as holographic phase retrieval is related to our approach as here a known reference signal is concatenated with ξ to facilitate the phase estimation [1]. Interference with known references for classical phase retrieval are also analyzed in [3, 11] for known (Fourier) operators.

A random projection setup similar to the one we consider has been used for classification [17]. However, in that work the phase is not determined and the measured absolute magnitudes are used. Certain applications in compressive imaging involve the calibration of the transmission matrix, though this process is impractical at high pixel counts [6, 14]. Another possibility is to directly estimate the inverse of the transmission matrix [9] for use with magnitude measurements. Recent work on imaging foregoes calibration by using convolutional neural networks [18]. Leaving

hardware implementations aside, there have been multiple algorithmic efforts to improve the speed of random projections [12, 24].

2 The measurement phase retrieval problem

We will denote the signal of interest by $\boldsymbol{\xi} \in \mathbb{R}^N$, and the K reference *anchor* signals by $\mathbf{r}_k \in \mathbb{R}^N$ for $1 \leq k \leq K$. To present the full algorithm we will need to use multiple signals of interest which we will then denote $\boldsymbol{\xi}_1, \dots, \boldsymbol{\xi}_S$; each $\boldsymbol{\xi}_s$ is called a frame. We set the last, K th anchor to be the origin, $\mathbf{r}_K = \mathbf{0}$. We ascribe $\boldsymbol{\xi}$ and the anchors to the columns of the matrix $\mathbf{X} \in \mathbb{R}^{N \times Q}$, so that $\mathbf{X} = [\boldsymbol{\xi}, \mathbf{r}_1, \mathbf{r}_2, \dots, \mathbf{r}_K]$ and let $Q = K + 1$. The q th column of \mathbf{X} is denoted \mathbf{x}_q . For any $1 \leq q, r \leq Q$, we let $\mathbf{y}_q = \mathbf{A}\mathbf{x}_q$ and $\mathbf{y}_{qr} := \mathbf{A}(\mathbf{x}_q - \mathbf{x}_r)$, with $y_{qr,m}$ being its m th entry. Finally, the m th row of \mathbf{A} will be denoted by \mathbf{a}^m so that $y_{qr,m} = \langle \mathbf{a}^m, \mathbf{x}_q - \mathbf{x}_r \rangle$.

2.1 Problem statement and recovery up to a reference phase

Since we do not know \mathbf{A} , it is clear that recovering the absolute phase of $\mathbf{A}\boldsymbol{\xi}$ is impossible. On the other hand, many algorithms do not require any knowledge of \mathbf{A} except that it is iid standard complex Gaussian, and that it does not change throughout the computations.

Consider adding a constant phase to each row of \mathbf{A} . This can be modelled as multiplying \mathbf{A} by a diagonal phasing matrix $\boldsymbol{\Gamma} = \text{diag}(e^{j\phi_1}, \dots, e^{j\phi_m})$. Since a standard complex Gaussian is circularly symmetric, $\boldsymbol{\Gamma}\mathbf{A}$ has the same distribution as \mathbf{A} . Therefore, since we do not know \mathbf{A} , whether we are working with \mathbf{A} itself or with $\boldsymbol{\Gamma}\mathbf{A}$ for some possibly unknown $\boldsymbol{\Gamma}$ is irrelevant as long as the same *effective* $\boldsymbol{\Gamma}$ is used for all inputs during algorithm operation. In other words, the relative phase between the different frames does not depend on $\boldsymbol{\Gamma}$ and motivates the following problem statement:

Problem 1. *Given a collection of input frames $\boldsymbol{\xi}_1, \dots, \boldsymbol{\xi}_S$ to be randomly projected and a device illustrated in Figure 1 (left) with an unknown transmission matrix $\mathbf{A} \in \mathbb{C}^{M \times N}$ and a b -bit camera, compute the estimates of projections $\hat{\mathbf{y}}_1, \dots, \hat{\mathbf{y}}_S$ up to a global row-wise phase, that is, so that there exists some diagonal phasing matrix $\boldsymbol{\Gamma}$ such that $\hat{\mathbf{y}}_s \approx \boldsymbol{\Gamma}\mathbf{y}_s$ for all $1 \leq s \leq S$.*

2.2 MPR as a distance geometry problem

Since the rows of \mathbf{A} are statistically independent, we can explain our algorithm for a single row and then repeat the same steps for the remaining rows. We will therefore omit the row subscript/superscript m except where explicitly necessary.

Instead of randomly projecting $\boldsymbol{\xi}$ and measuring the corresponding projection magnitude $|\mathbf{A}\boldsymbol{\xi}|^2$, consider randomly projecting the difference between $\boldsymbol{\xi}$ and some reference vector, or more generally a difference between two columns in \mathbf{X} , thus measuring $|\langle \mathbf{a}, \mathbf{x}_q - \mathbf{x}_r \rangle|^2 = |y_q - y_r|^2$. Interpreting y_q and y_r as points in the complex plane, we see that the camera sensor measures exactly the squared Euclidean distance between them. Since we control the input to the OPU, we can indeed set it to $\mathbf{x}_q - \mathbf{x}_r$ and measure $|y_q - y_r|^2$ for all $1 \leq q, r \leq Q$.

This is the key point: as we can measure pairwise distances between a collection of two-dimensional vectors in the two-dimensional complex plane, we can use established distance geometry algorithms such as multidimensional scaling (MDS) to localize points and get their phase. This is illustrated in Figure 1 (right). The same figure also illustrates the well known fact that rigid transformations of a

point set cannot be recovered from distance data. We need to worry about two things: translations and rotations.

The translation ambiguity can be easily dealt with if one notes that for any column \mathbf{x}_q of \mathbf{X} , $|y_q| = |\langle \mathbf{a}, \mathbf{x}_q \rangle|$ gives us the distance of y_q to the origin which is a fixed point, ultimately resolving the translation ambiguity. There is, however, no similar simple way to do away with the rotation ambiguity, so it might seem that there is no way to uniquely determine the phase of $\langle \mathbf{a}, \boldsymbol{\xi} \rangle$. This is where the discussion from the preceding subsection comes to the rescue. Since $\boldsymbol{\Gamma}$ is arbitrary, as long as it is fixed for all the frames, we can arbitrarily set the phase of any given frame and use it as a phase reference, making sure that the relative phases are computed correctly.

2.3 Proposed algorithm

As defined previously, the columns of $\mathbf{X} \in \mathbb{R}^{N \times Q}$ list the signal of interest and the anchors. Recall that all the entries of \mathbf{X} are known. Using the OPU, we can compute a noisy (quantized) version of

$$|y_{qr}|^2 = |\langle \mathbf{a}, \mathbf{x}_q - \mathbf{x}_r \rangle|^2 = |y_q - y_r|^2, \quad (3)$$

for all (q, r) , which gives us $Q(Q-1)/2$ squared Euclidean distances between points $\{y_q \in \mathbb{C}\}_{q=1}^Q$ on the complex plane. These distances can be used to populate a Euclidean (squared) distance matrix $\mathbf{D} \in \mathbb{R}^{Q \times Q}$ as $\mathbf{D} = (d_{qr}^2)_{q,r=1}^Q = (|y_{qr}|^2)_{q,r=1}^Q$, which we will use to localize the y_q .

We start by defining the matrix of points in \mathbb{R}^2 as

$$\boldsymbol{\Upsilon} = \begin{bmatrix} \text{Re}(y_1) & \text{Re}(y_2) & \cdots & \text{Re}(y_Q) \\ \text{Im}(y_1) & \text{Im}(y_2) & \cdots & \text{Im}(y_Q) \end{bmatrix} \in \mathbb{R}^{2 \times Q}.$$

Denoting the q th column of $\boldsymbol{\Upsilon}$ by \mathbf{v}_q , we have $d_{qr}^2 = \|\mathbf{v}_q - \mathbf{v}_r\|_2^2 = \mathbf{v}_q^T \mathbf{v}_q - 2\mathbf{v}_q^T \mathbf{v}_r + \mathbf{v}_r^T \mathbf{v}_r$ so that

$$\mathbf{D} = \text{diag}(\mathbf{G}) \mathbf{1}_Q^T - 2\mathbf{G} + \mathbf{1}_Q \text{diag}(\mathbf{G})^T =: \mathcal{K}(\mathbf{G}), \quad (4)$$

where $\text{diag}(\mathbf{G}) \in \mathbb{R}^Q$ is the vector of the diagonal entries in $\mathbf{G} := \boldsymbol{\Upsilon}^T \boldsymbol{\Upsilon} \in \mathbb{R}^{Q \times Q}$ and $\mathbf{1}_Q \in \mathbb{R}^Q$ is the vector of Q ones. We denote by \mathbf{J} the geometric centering matrix, $\mathbf{J} := \mathbf{I} - \frac{1}{Q} \mathbf{1}_Q \mathbf{1}_Q^T$ so that

$$\widehat{\mathbf{G}} = -\frac{1}{2} \mathbf{J} \mathbf{D} \mathbf{J} = \mathbf{J} \mathbf{G} \mathbf{J} = (\boldsymbol{\Upsilon} \mathbf{J})^T (\boldsymbol{\Upsilon} \mathbf{J})$$

is the Gram matrix of the centered point set in $\boldsymbol{\Upsilon}$. An estimate $\widehat{\boldsymbol{\Upsilon}}$ of the centered point set is then obtained by eigendecomposition as $\widehat{\mathbf{G}} = \mathbf{V} \text{diag}(\lambda_1, \dots, \lambda_Q) \mathbf{V}^T$ and taking $\widehat{\boldsymbol{\Upsilon}} = [\sqrt{\lambda_1} \mathbf{v}_1, \sqrt{\lambda_2} \mathbf{v}_2]^T$, assuming that the eigenvalue sequence is non-increasing. This localization process is the classical MDS algorithm [22, 5]. Finally, the phases can be calculated via a four-quadrant inverse tangent, $\phi(y_q) = \arctan(v_{q2}, v_{q1})$.

Procrustes analysis. The point set recovered via the described MDS will have its centroid at the origin. This is a consequence of the used algorithm, and not the “true” origin. As described above, we know that $|y_q|^2$ define squared distances to the origin and $y_Q = \langle \mathbf{a}, \mathbf{x}_Q \rangle = 0 + 0j$, meaning that we can recover the correct origin by translating the point set by $-\mathbf{v}_Q$.

The correct absolute rotation cannot be recovered. However, since we only care about working with some effective $\boldsymbol{\Gamma} \mathbf{A}$ with the correct distribution, we only need to ensure that the relative phases

between the different frames are correct. We can thus designate the first frame as the reference frame and choose the rotation (which directly corresponds to the phase) arbitrarily. Once this rotation is chosen, the anchors $\mathbf{r}_1, \dots, \mathbf{r}_K$ are fixed, which in turn fixes the diagonal phasing matrix $\mathbf{\Gamma}$.

Since \mathbf{A} is unknown, $\mathbf{\Gamma}$ is also unknown, but fixed anchors will allow us to compute the correct relative phase with respect to $\mathbf{\Gamma}\mathbf{A}$ for the subsequent inputs. Namely, upon receiving a new input ξ_s to be randomly projected, we now localize it with respect to a fixed set of anchors. This is achieved by Procrustes analysis. Denoting by $\tilde{\mathbf{Y}}_1$ our reference estimate of the anchor positions in frame 1 (columns 2– Q of $\tilde{\mathbf{Y}}$), and by $\tilde{\mathbf{Y}}_s$ the MDS estimate of anchor positions in frame s (adequately translated). Let $\tilde{\mathbf{Y}}_s \tilde{\mathbf{Y}}_1^T = \mathbf{U}\mathbf{\Sigma}\mathbf{V}^T$ be the singular value decomposition of $\tilde{\mathbf{Y}}_s \tilde{\mathbf{Y}}_1^T$. The optimal rotation matrix (in the least squares sense) is then $\mathbf{R} = \mathbf{V}\mathbf{U}^T$ so that $\mathbf{R}\tilde{\mathbf{Y}}_s \approx \tilde{\mathbf{Y}}_1$ [19].

Finally, we note that with a good estimate of anchors, one can imagine not relocalizing them in every frame. The localization problem for ξ then boils down to multilateration, cf. Section C in the supplementary material.

2.4 Sensitivity threshold and missing measurements

As we further elaborate in Section A of the supplementary material, in practice some measurements fall below the sensitivity threshold of the camera and produce spurious values. A nice benefit of multiple “views” of ξ via its interaction with reference signals is that we can ignore those measurements. This introduces missing values in \mathbf{D} which can be modeled via a binary mask matrix \mathbf{W} . The recovery problem can be modeled as estimating \mathbf{Y} from $\mathbf{W} \odot (\mathbf{D} + \mathbf{E})$ where $\mathbf{W} \in \mathbb{R}^{N \times N}$ contains zeros for the entries which fall below some prescribed threshold, and ones otherwise.

We can predict the performance of the proposed method when modeling the entries of \mathbf{W} as iid Bernoulli random variables with parameter p , where $1 - p$ is the probability that an entry falls below the sensitivity threshold and \mathbf{E} as uniform quantization noise distributed as $\mathcal{U}\left(-\frac{\kappa}{2(2^b-1)}, \frac{\kappa}{2(2^b-1)}\right)$, where b is the number of bits, and κ an upper bound on the entries of \mathbf{D} (in our case $2^8 - 1 = 255$).

Adapting existing results on the performance of multidimensional scaling [27] (by noting that \mathbf{E} is sub-Gaussian), we can get the following scaling of the distance recovery error with the number of anchors K (for K sufficiently large),

$$\frac{1}{K} \mathbb{E} \left[\left\| \hat{\mathbf{D}} - \mathbf{D} \right\|_F \right] \lesssim \frac{\kappa}{\sqrt{pK}}, \quad (5)$$

where \lesssim denotes inequality up to a constant which depends on the number of bits b , the sub-Gaussian norm of the entries in \mathbf{E} , and the dimension of the ambient space (here \mathbb{R}^2). An important implication is that even for coarse quantization (small b) and for a large fraction of entries below the sensitivity threshold (small p), we can achieve arbitrarily small amplitude and phase errors *per point* by increasing the number of reference signals K .

Refinement with gradient descent. The output of the classical MDS method described above can be further refined via a local search. A standard differentiable objective called the squared stress is defined as follows,

$$\min_{\mathbf{Z}} f(\mathbf{Y}) = \min_{\mathbf{Z}} \left\| \mathbf{W} \odot \left(\mathbf{D} - \mathcal{K}(\mathbf{Z}^T \mathbf{Z}) \right) \right\|_F^2, \quad (6)$$

Algorithm 1 MPR algorithm for S frames.

Input: Squared distances $[|y_{jQ,m} - y_{lQ,m}|^2]_s$ for all $1 \leq j, l \leq Q$ for frames $1 \leq s \leq S$ and rows $1 \leq m \leq M$; $[\cdot]_s$ denotes frame s

Output: $\mathbf{Y} \in \mathbb{C}^{M \times S}$ containing all localized points such that $\mathbf{y}_s = \mathbf{\Gamma} \mathbf{A} \boldsymbol{\xi}_s$ for some fixed $\mathbf{\Gamma}$

```

1:  $\mathbf{Y} \leftarrow \mathbf{0}_{M \times S}$  ▷ Initialize  $\mathbf{Y}$ 
2:  $m \leftarrow 1$ 
3: while  $m \leq M$  do ▷ Solve each row separately
4:   Populate all frame  $s = 1$  distances into distance matrix  $\mathbf{D}$  ▷  $\mathbf{D} \in \mathbb{R}^{Q \times Q}$ 
5:    $[\mathbf{Y}]_1 \leftarrow \text{MDS}(\mathbf{D})$  ▷  $[\mathbf{Y}]_1 \in \mathbb{R}^{2 \times Q}$ 
6:    $[\mathbf{Y}]_1 \leftarrow \text{GradientDescent}(\mathbf{D}, [\mathbf{Y}]_1)$ 
7:    $[\mathbf{Y}]_1 \leftarrow [\mathbf{Y}]_1 - [\mathbf{v}_Q]_1 \mathbf{1}^T$  ▷ Translate to align with origin
8:    $s \leftarrow 2$ 
9:   while  $s \leq S$  do
10:    Populate all frame  $s$  distances into distance matrix  $\mathbf{D}$ 
11:     $[\mathbf{Y}]_s \leftarrow \text{MDS}(\mathbf{D})$ 
12:     $[\mathbf{Y}]_s \leftarrow \text{GradientDescent}(\mathbf{D}, [\mathbf{Y}]_s)$ 
13:     $[\mathbf{Y}]_s \leftarrow [\mathbf{Y}]_s - [\mathbf{v}_Q]_s \mathbf{1}^T$ 
14:     $\mathbf{R} \leftarrow \text{Procrustes}([\mathbf{v}_2, \dots, \mathbf{v}_Q]_1, [\mathbf{v}_2, \dots, \mathbf{v}_Q]_s)$  ▷  $\mathbf{R}$  aligns frames 1 and  $s$  anchors
15:     $[\mathbf{Y}]_s \leftarrow \text{Align}([\mathbf{Y}]_s, \mathbf{R}, [\mathbf{v}_2, \dots, \mathbf{v}_Q]_1)$  ▷ Align anchors
16:     $s \leftarrow s + 1$ 
17:  end while
18:   $\mathbf{U} \leftarrow [[\mathbf{v}_1]_1, [\mathbf{v}_1]_2, \dots, [\mathbf{v}_1]_S]$  ▷  $\mathbf{U} \in \mathbb{R}^{2 \times S}$ 
19:   $\mathbf{y}^m \leftarrow \mathbf{u}^1 + j\mathbf{u}^2$  ▷ Multiply second row of  $\mathbf{U}$  with  $j$  and add to first row
20:   $m \leftarrow m + 1$ 
21: end while

```

where $\mathcal{K}(\cdot)$ is as defined in (4) and $\mathbf{Z} \in \mathbb{R}^{2 \times Q}$ is the point matrix induced by row m of \mathbf{A} . In our experiments we report the result of refining the classical MDS results via gradient descent on (6).

Note that the optimization (6) is nonconvex. The complete procedure is thus analogous to the what has by now become standard in non-convex phase retrieval by spectral initialization followed by gradient descent [15, 4]. Algorithm 1 summarizes our proposed method.

3 Experimental verification and application

We test the proposed MPR algorithm via simulations and experiments on a real OPU. For hardware experiments, we use a scikit-learn interface to a publicly available cloud-based OPU.¹

Evaluation metrics. The main challenge is to evaluate the performance without knowing the transmission matrix \mathbf{A} . To this end, we propose to use the *linearity error*. The rationale behind this metric is that with the phase correctly recovered, the end-to-end system should be linear. That is, if we recover \mathbf{y} and \mathbf{z} from $|\mathbf{y}|^2 = |\mathbf{A}\boldsymbol{\xi}_1|^2$ and $|\mathbf{z}|^2 = |\mathbf{A}\boldsymbol{\xi}_2|^2$, then we should get $(\mathbf{y} + \mathbf{z})$ when applying

¹<https://www.lighton.ai/lighton-cloud/>.

Reproducible code available at https://github.com/swing-research/opu_phase under the MIT License.

the method to $|v|^2 = |\mathbf{A}(\boldsymbol{\xi}_1 + \boldsymbol{\xi}_2)|^2$. With this notation, the relative linearity error is defined as

$$\text{linearity error} = \frac{1}{M} \sum_{m=1}^M \frac{|(y_m + z_m) - v_m|}{|v_m|}. \quad (7)$$

The second metric we use is the number of “good” or correct bits. This metric can only be evaluated in simulation since it requires the knowledge of the ground truth measurements. Letting $|y|^2 = |\langle \mathbf{a}, \boldsymbol{\xi} \rangle|^2$ and \hat{y} be our estimate of y , the number of good bits is defined as

$$\text{good bits} = -\frac{20}{6.02} \log \left(\frac{||y|^2 - |\hat{y}|^2|}{|y|^2} \right).$$

It is proportional to the signal-to-quantization-noise ratio if the distances uniformly cover all quantization levels.²

3.1 Experiments

In all simulations, intensity measurements are quantized to 8 bits and all signals and references are iid standard (complex) Gaussian random vectors.

We first test the phase recovery performance by evaluating the linearity error. In simulation, we draw random frames $\boldsymbol{\xi}_1$, $\boldsymbol{\xi}_2$, and $\mathbf{A} \in \mathbb{C}^{100 \times 64^2}$. We apply Algorithm 1 to $|\mathbf{A}\boldsymbol{\xi}_1|^2$, $|\mathbf{A}\boldsymbol{\xi}_2|^2$ and $|\mathbf{A}(\boldsymbol{\xi}_1 + \boldsymbol{\xi}_2)|^2$ and calculate the linearity error (7). We use classical MDS and MDS with gradient descent (MDS-GD). Figure 2a shows that the system is indeed approximately linear and that the linearity error becomes smaller as the number of reference signals grows. In Figure 2b, we set the sensitivity threshold to $\tau = 6$ and zero the distances below the threshold per (2). Again, the linearity error quickly becomes small as the number of anchors increases showing that the overall system is robust and that it allows recovery of phase for small-intensity signals.

Next, we test the linearity error with a real hardware OPU. The OPU gives 8-bit unsigned integer measurements. A major challenge is that since the DMD is binary, the inputs need to be binary. This imposes restrictions on reference design. Section A in the supplementary material describes how we create binary references and addresses other hardware-related practicalities.

Figure 2c reports the linearity error on the OPU with suitably designed references. The empirically determined sensitivity threshold of the camera is $\tau = 6$, and the measurements below the threshold were not used. We ignore rows of \mathbf{A} which give points with small norms (less than two) because they are prone to noise and disproportionately influence the relative error. Once again, we observe that the end-to-end system with Algorithm 1 is approximately linear and that the linearity improves with increasing number of anchors.

Finally, we demonstrate the magnitude denoising performance. We draw $\mathbf{a} \in \mathbb{C}^{100}$, a random signal $\boldsymbol{\xi} \in \mathbb{R}^{100}$ and a set of random reference anchor signals. We run our algorithm for number of anchors varying between 2 and 15. For each number of anchors, we recover \hat{y} for $|y|^2 = |\langle \mathbf{a}, \boldsymbol{\xi} \rangle|^2$ using either classical MDS or MDS-GD. We then measure the number of good bits. The average results over 100 trials are shown in Figure 3a. Figure 3b reports the same experiment with the sensitivity threshold set to $\tau = 6$ (that is, the entries below τ are zeroed in the distance matrix per (2)). Both figures show that the proposed algorithm significantly improves the estimated magnitudes in addition to recovering the phases.

²Note that the quantity registered by the camera is actually the squared magnitude, hence the factor 20.

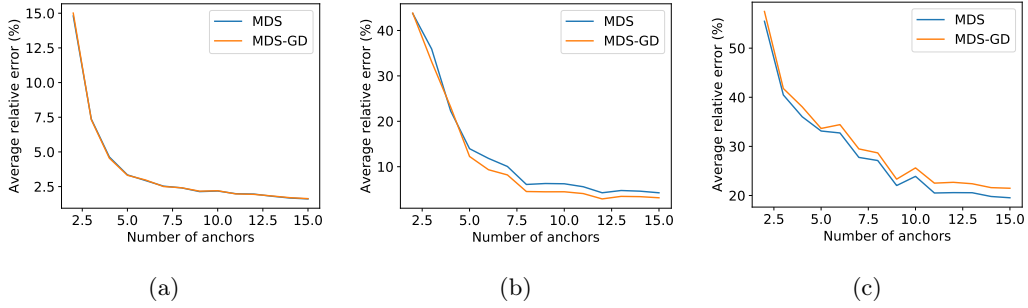


Figure 2: Linearity error experiments. (a) In simulation; (b) In simulation with $\tau = 6$; (c) On the OPU. In all cases the error decreases as the number of anchors increases.

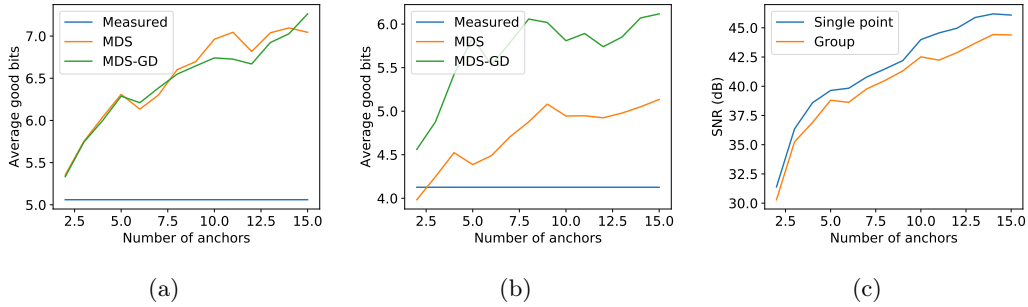


Figure 3: (a) Magnitude denoising performance of MDS and MDS-GD; (b) Magnitude denoising performance with $\tau = 6$; (c) SR-LS is used to locate a single point when anchors are known and MDS is used to locate all points when anchors are unknown.

We also test a scenario where the anchor positions on the complex plane are known exactly. Multilateration is performed by minimizing SR-LS objective (see (8) in the supplementary material). Experimental setting is the same as in the “good bits” experiment and we calculate the SNR of the recovered complex points. Figure 3c shows that although having perfect knowledge of anchor locations helps, classical MDS alone does not perform much worse.

Optical randomized singular value decomposition. We use the OPU and Algorithm 1 to implement randomized singular value decomposition (RSVD) described in [8]. We use 5 anchors in all RSVD experiments. The original algorithm and the OPU RSVD variant with some adaptations are described in Algorithms 2 and 3 in the supplementary material.

The RSVD algorithm for an input matrix $\mathbf{B} \in \mathbb{R}^{M \times N}$ requires the computation of $\mathbf{B}\mathbf{\Omega}$ where $\mathbf{\Omega} \in \mathbb{R}^{N \times 2K}$ is a standard Gaussian matrix, K is the target number of singular vectors, and $2K$ may be interpreted as the number of projections for each row of \mathbf{B} . An interesting observation is that since we recover multiplications by a complex matrix, we can halve the number of projections with the OPU with respect to the original algorithm. By treating each row of \mathbf{B} as an input frame, we obtain $\mathbf{Y} \in \mathbb{C}^{K \times M}$ when $|\mathbf{Y}|^2 = |\mathbf{A}\mathbf{B}^T|^2$ via Algorithm 1, where \mathbf{A} has K rows. Then, computing

$\mathbf{P} = [\text{Re}(\mathbf{Y}^*) \quad \text{Im}(\mathbf{Y}^*)] \in \mathbb{R}^{M \times 2K}$ is equivalent to computing $\mathbf{B}\mathbf{\Omega}$ for a real $\mathbf{\Omega}$. Section B in the supplementary material describes this in more detail.

Figure 4 (left) reports experiments with $\mathbf{B} \in \mathbb{R}^{10 \times 10^4}$, different numbers of random projections, and ten trials per number of projections. We plot the average error per entry when reconstructing \mathbf{B} from its RSVD. Next, we take 500 28×28 samples from the MNIST dataset [13], threshold them to binary values, vectorize, and stack in a matrix $\mathbf{B} \in \mathbb{R}^{500 \times 28^2}$. Figure 4 (right) shows the seven leading right singular vectors reshaped to 28×28 . The error is negligible.

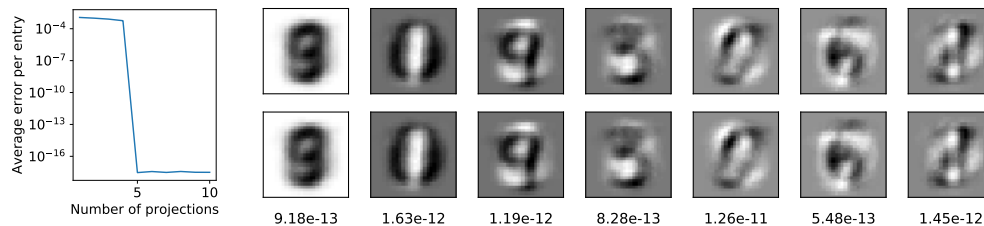


Figure 4: Left: RSVD error with varying number of projections on hardware; right: The top rows shows the leading right singular vectors of an MNIST matrix after performing RSVD with the OPU and using our algorithm. The bottom row shows the leading right singular vectors from Python. The relative error is below each singular vector.

4 Conclusion

Traditional computation methods are often too slow for many processing tasks which involve large data streams. This motivates alternatives which instead use fast physics to “compute” the desired functions. In this work, we looked at using optics and multiple scattering media to obtain linear random projections. A common difficulty with optical systems is that off-the-shelf camera sensors only register the intensity of the scattered light. Our results show that there is nevertheless no need to reach for more complicated and more expensive coherent setups. We showed that measurement phase retrieval can be cast as a problem in distance geometry, and that the unknown phase of random projections can be recovered even without knowing the transmission matrix of the medium.

Simulations and experiments on real hardware show that the OPU setup combined with our algorithm indeed approximates an end-to-end linear system. What is more, we also improve intensity measurements. The fact that we get full complex measurements allows us to implement a whole new spate of randomized algorithms; we demonstrated the potential by the randomized singular value decomposition. These benefits come at the expense of a reduction in data throughput. Future work will have to precisely quantify the smallest achievable data rate reduction due to allocating a part of the duty cycle for reference measurements. Since the optical processing data rates are very high to begin with, we expect the bottlenecks to appear elsewhere.

References

- [1] David A Barmherzig, Ju Sun, Emmanuel J Candes, TJ Lane, and Po-Nan Li. Holographic phase retrieval and optimal reference design. *arXiv preprint arXiv:1901.06453*, 2019.
- [2] Amir Beck, Petre Stoica, and Jian Li. Exact and approximate solutions of source localization problems. *IEEE Transactions on Signal Processing*, 56(5):1770–1778, 2008.
- [3] Robert Beinert. One-dimensional phase retrieval with additional interference intensity measurements. *Results in Mathematics*, 72(1-2):1–24, 2017.
- [4] Emmanuel J Candes, Xiaodong Li, and Mahdi Soltanolkotabi. Phase retrieval via wirtinger flow: Theory and algorithms. *IEEE Transactions on Information Theory*, 61(4):1985–2007, 2015.
- [5] Ivan Dokmanic, Reza Parhizkar, Juri Ranieri, and Martin Vetterli. Euclidean distance matrices: essential theory, algorithms, and applications. *IEEE Signal Processing Magazine*, 32(6):12–30, 2015.
- [6] Angélique Drémeau, Antoine Liutkus, David Martina, Ori Katz, Christophe Schülke, Florent Krzakala, Sylvain Gigan, and Laurent Daudet. Reference-less measurement of the transmission matrix of a highly scattering material using a dmd and phase retrieval techniques. *Optics express*, 23(9):11898–11911, 2015.
- [7] James R Fienup. Phase retrieval algorithms: a comparison. *Applied optics*, 21(15):2758–2769, 1982.
- [8] Nathan Halko, Per-Gunnar Martinsson, and Joel A Tropp. Finding structure with randomness: Probabilistic algorithms for constructing approximate matrix decompositions. *SIAM review*, 53(2):217–288, 2011.
- [9] Ryoichi Horisaki, Ryosuke Takagi, and Jun Tanida. Learning-based imaging through scattering media. *Optics express*, 24(13):13738–13743, 2016.
- [10] Kishore Jaganathan, Yonina C Eldar, and Babak Hassibi. Phase retrieval: An overview of recent developments. *arXiv preprint arXiv:1510.07713*, 2015.
- [11] Wooshik Kim and Monson H Hayes. Phase retrieval using two fourier-transform intensities. *JOSA A*, 7(3):441–449, 1990.
- [12] Quoc Le, Tamás Sarlós, and Alex Smola. Fastfood-approximating kernel expansions in loglinear time. 2013.
- [13] Yann LeCun, Léon Bottou, Yoshua Bengio, Patrick Haffner, et al. Gradient-based learning applied to document recognition. *Proceedings of the IEEE*, 86(11):2278–2324, 1998.
- [14] Antoine Liutkus, David Martina, Sébastien Popoff, Gilles Chardon, Ori Katz, Geoffroy Lerosey, Sylvain Gigan, Laurent Daudet, and Igor Carron. Imaging with nature: Compressive imaging using a multiply scattering medium. *Scientific reports*, 4:5552, 2014.
- [15] Praneeth Netrapalli, Prateek Jain, and Sujay Sanghavi. Phase retrieval using alternating minimization. In *Advances in Neural Information Processing Systems*, pages 2796–2804, 2013.

- [16] Ali Rahimi and Benjamin Recht. Random features for large-scale kernel machines. In *Advances in Neural Information Processing Systems*, pages 1177–1184, 2008.
- [17] Alaa Saade, Francesco Caltagirone, Igor Carron, Laurent Daudet, Angélique Drémeau, Sylvain Gigan, and Florent Krzakala. Random projections through multiple optical scattering: Approximating kernels at the speed of light. In *2016 IEEE International Conference on Acoustics, Speech and Signal Processing (ICASSP)*, pages 6215–6219. IEEE, 2016.
- [18] Guy Satat, Matthew Tancik, Otkrist Gupta, Barmak Heshmat, and Ramesh Raskar. Object classification through scattering media with deep learning on time resolved measurement. *Optics express*, 25(15):17466–17479, 2017.
- [19] Peter Hans Schoenemann. *A solution of the orthogonal Procrustes problem with applications to orthogonal and oblique rotation*. PhD thesis, University of Illinois at Urbana-Champaign, 1964.
- [20] Yoav Shechtman, Yonina C Eldar, Oren Cohen, Henry Nicholas Chapman, Jianwei Miao, and Mordechai Segev. Phase retrieval with application to optical imaging: a contemporary overview. *IEEE signal processing magazine*, 32(3):87–109, 2015.
- [21] Petre Stoica and Jian Li. Lecture notes-source localization from range-difference measurements. *IEEE Signal Processing Magazine*, 23(6):63–66, 2006.
- [22] Warren S Torgerson. Multidimensional scaling: I. theory and method. *Psychometrika*, 17(4):401–419, 1952.
- [23] Joel A Tropp, Alp Yurtsever, Madeleine Udell, and Volkan Cevher. Practical sketching algorithms for low-rank matrix approximation. *SIAM Journal on Matrix Analysis and Applications*, 38(4):1454–1485, 2017.
- [24] Yun Yang, Mert Pilanci, Martin J Wainwright, et al. Randomized sketches for kernels: Fast and optimal nonparametric regression. *The Annals of Statistics*, 45(3):991–1023, 2017.
- [25] Felix Xinnan X Yu, Ananda Theertha Suresh, Krzysztof M Choromanski, Daniel N Holtmann-Rice, and Sanjiv Kumar. Orthogonal random features. In *Advances in Neural Information Processing Systems*, pages 1975–1983, 2016.
- [26] Alp Yurtsever, Madeleine Udell, Joel A Tropp, and Volkan Cevher. Sketchy decisions: Convex low-rank matrix optimization with optimal storage. *arXiv preprint arXiv:1702.06838*, 2017.
- [27] Huan Zhang, Yulong Liu, and Hong Lei. Localization from incomplete euclidean distance matrix: Performance analysis for the svd-mds approach. *IEEE Transactions on Signal Processing*, 2019.

Supplementary material

A Practical considerations with hardware

Reference design. On the OPU system described in Figure 1 we can only encode and randomly project binary signals. Therefore, all pairwise differences $(\mathbf{x}_q - \mathbf{x}_r)$ between the columns of $\mathbf{X} \in \mathbb{R}^{N \times Q}$ must be binary. To design reference signals we first collect all frames $\{\boldsymbol{\xi}_s\}_{s=1}^S$ and sum them $\sum_{s=1}^S \boldsymbol{\xi}_s$. The first reference \mathbf{r}_1 is initialized to ones at the indices where $\sum_{s=1}^S \boldsymbol{\xi}_s$ is nonzero. Next, some of \mathbf{r}_1 's zero-valued entries are flipped to one with probability α . A similar process is used for all subsequent references. In general, a reference \mathbf{r}_q is initialized by assigning ones to the nonzero support of $(\sum_{s=1}^S \boldsymbol{\xi}_s + \sum_{k=1}^{q-1} \mathbf{r}_k)$ and then flipping some of its zero entries with probability α .

There is a tradeoff between large and small α . If α is too large, a reference may become all-ones before all subsequent references are generated. On the other hand if α is too small, $\mathbf{r}_{q+1} - \mathbf{r}_q$ will have many zeros and so $|\mathbf{A}(\mathbf{r}_{q+1} - \mathbf{r}_q)|^2$ may not be high enough to be detected by the camera sensor. The consequence of this tradeoff is that in practice the number of anchors is limited. Furthermore, in general a larger N makes it easier to make K good anchors as α can be larger which keeps $|\mathbf{A}(\mathbf{r}_{q+1} - \mathbf{r}_q)|^2$ away from the sensitivity threshold.

Figure 5 shows binary references reshaped into squares which were used for the linearity experiment on the OPU in Figure 2c. Here, $N = 64^2$ and $\alpha = 0.2$. The number on top of each reference is the difference in the number of ones between itself and the previously generated reference.

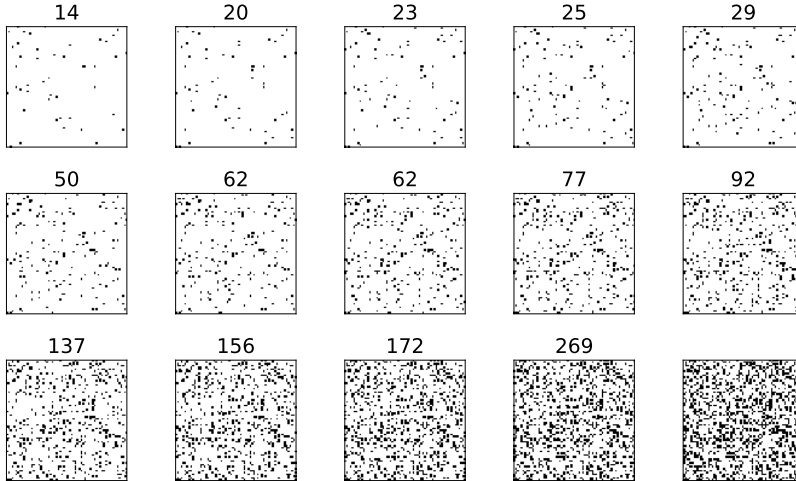


Figure 5: Binary references reshaped into squares which were used for the linearity experiment on the OPU in Figure 2c. Here $N = 64^2$ and $\alpha = 0.2$. The number on top of each anchor is the difference in the number of ones between itself and the previously generated reference.

Minimum attainable measurement. To determine the sensitivity threshold τ , we randomly project an all-zero signal a few times and record the output. The minimum, mode or mean of these measurements can be taken to be the minimum that can be measured. Once τ is estimated, we apply a mask and zero any measurements which are equal to or less than the minimum.

Camera sensor saturation. It is possible for the signal reaching the camera to saturate the sensor. In a b -bit system we can detect this if many measurements are equal to $2^b - 1$. In all experiments we ensure that there is no saturation by adjusting the camera exposure. This again involves a tradeoff: if exposure is too high, we saturate the sensor; if it is too low, measurements may be too small to be detected and we are not exploiting the full dynamic range.

B Randomized singular value decomposition (RSVD) details

Algorithm 2 is the prototype randomized SVD algorithm given by [8]. To implement this on hardware we replace Step 1 and 2 to formulate Algorithm 3. As \mathbf{A} in Algorithm 3 has iid entries following a standard complex Gaussian, calculating \mathbf{P} in Algorithm 3 is the same as doing step 2 in Algorithm 2. We only need to do half the number of projections because we use an iid complex random matrix. The real and imaginary parts are two random projections.

Algorithm 2 Prototype randomized SVD algorithm [8].

Input: Matrix, $\mathbf{B} \in \mathbb{R}^{M \times N}$ whose SVD is required, a target number of K singular vectors

Output: The SVD \mathbf{U} , $\mathbf{\Sigma}$ and \mathbf{V}^*

- 1: Generate an $N \times 2K$ random Gaussian matrix \mathbf{A} .
 - 2: Form $\mathbf{Y} = \mathbf{B}\mathbf{A}$.
 - 3: Construct a matrix \mathbf{Q} whose columns form an orthonormal basis for the range of \mathbf{Y} .
 - 4: Form $\mathbf{C} = \mathbf{Q}^* \mathbf{B}$.
 - 5: Compute the SVD of the smaller $\mathbf{C} = \tilde{\mathbf{U}} \mathbf{\Sigma} \mathbf{V}^*$.
 - 6: $\mathbf{U} = \mathbf{Q} \tilde{\mathbf{U}}$.
-

Algorithm 3 Randomized SVD algorithm on the OPU.

Input: Matrix, $\mathbf{B} \in \mathbb{R}^{M \times N}$ whose SVD is required, a target number of K singular vectors

Output: The SVD \mathbf{U} , $\mathbf{\Sigma}$ and \mathbf{V}^*

- 1: Solve $|\mathbf{Y}|^2 = |\mathbf{A}\mathbf{B}^*|^2$ by treating each column of \mathbf{B}^* as a frame and using Algorithm 1, where \mathbf{A} is as in the MPR problem and has K rows.
 - 2: Horizontally stack the real and imaginary parts of $\mathbf{Y}^* \in \mathbb{C}^{M \times K}$ as $\mathbf{P} = [\text{Re}(\mathbf{Y}^*) \quad \text{Im}(\mathbf{Y}^*)] \in \mathbb{R}^{M \times 2K}$.
 - 3: Construct a matrix \mathbf{Q} whose columns form an orthonormal basis for the range of \mathbf{P} .
 - 4: Form $\mathbf{C} = \mathbf{Q}^* \mathbf{B}$.
 - 5: Compute the SVD of the smaller $\mathbf{C} = \tilde{\mathbf{U}} \mathbf{\Sigma} \mathbf{V}^*$.
 - 6: $\mathbf{U} = \mathbf{Q} \tilde{\mathbf{U}}$.
-

C Localization with known anchor positions

If we have perfect knowledge of the anchor locations in the complex plane, we do not need to localize them for each frame s . The localization problem then boils down to multilateration, which can be formulated by minimizing the square-range-based least squares (SR-LS) objective [2],

$$\hat{\mathbf{v}}_1 = \min_{\mathbf{v}_1} \sum_{q=2}^Q \left(\|\mathbf{v}_1 - \mathbf{v}_q\|_2^2 - d_q^2 \right)^2 \quad (8)$$

where \mathbf{v}_q is as defined in Section 2.3 and d_k is the noisy measured distance. There exist efficient algorithms which solve (8) to global optimality [2], as well as suboptimal solutions based on solving a small linear system [21].